

Role of Al Vacancies in Thermodynamic Stability and Elastic Properties of AlB₂-type (Ta,Al)B₂: A First-Principles Study

Annop Ektarawong, Chayanon Atthapak and Björn Alling

The self-archived postprint version of this journal article is available at Linköping University Institutional Repository (DiVA):

<https://urn.kb.se/resolve?urn=urn:nbn:se:liu:diva-206362>

N.B.: When citing this work, cite the original publication.

Ektarawong, A., Atthapak, C., Alling, B., (2024), Role of Al Vacancies in Thermodynamic Stability and Elastic Properties of AlB₂-type (Ta,Al)B₂: A First-Principles Study, *Advanced Theory and Simulations*, 7(10), 2400421. <https://doi.org/10.1002/adts.202400421>

Original publication available at:

<https://doi.org/10.1002/adts.202400421>

Copyright: Wiley

<https://www.wiley.com/en-gb>

Role of Al vacancies in thermodynamic stability and elastic properties of AlB_2 -type $(\text{Ta},\text{Al})\text{B}_2$: A first-principles study

A. Ektarawong,^{1,2,3,*} C. Atthapak,^{1,2} and B. Alling⁴

¹*Extreme Conditions Physics Research Laboratory and Center of Excellence in Physics of Energy Materials (CE:PEM), Department of Physics, Faculty of Science, Chulalongkorn University, Bangkok 10330, Thailand*

²*Thailand Center of Excellence in Physics, Ministry of Higher Education, Science, Research and Innovation, 328 Si Ayutthaya Road, Bangkok 10400, Thailand*

³*Chula Intelligent and Complex Systems, Department of Physics, Faculty of Science, Chulalongkorn University, Bangkok 10330, Thailand*

⁴*Theoretical Physics Division, Department of Physics, Chemistry and Biology (IFM), Linköping University, SE-581 83, Linköping, Sweden*

AlB_2 -type TaB_2 is one of the transition-metal diborides, a class of refractory ceramics, that has increasingly received attention due particularly to their potential for hard-coating applications. In this work, we perform the first-principles calculations, in combination with the cluster-expansion method, to investigate the effect of mixing AlB_2 with TaB_2 on the thermodynamic stability, structural parameters, electronic density of states, and mechanical behavior of the resulting $(\text{Ta},\text{Al})\text{B}_2$ solid solutions. We find that the solid solutions display the chemical ordering of Ta and Al atoms both residing on the metal sublattice of the material, together with the preference for partial substitution of vacancies for Al atoms. This results in the formation of Al-deficient $(\text{Ta},\text{Al})\text{B}_2$ with the chemical composition $\text{Ta}_{0.6}\text{Al}_{0.3}\text{B}_2$, predicted to be thermodynamically stable even at absolute zero in the ternary Ta–Al–B system. We further find that such formation of Al vacancies in $(\text{Ta},\text{Al})\text{B}_2$ not only enhances the stability of the solutions but also improves their elastic properties and hardness, both of which could be attributed to the effect of electronic band filling. This investigation indeed sheds light on the interplay between the mixing of Ta and Al atoms and the presence of Al vacancies on the alloying and mechanical behaviors of $(\text{Ta},\text{Al})\text{B}_2$, and it thus offers valuable insights for further research and development of these ceramics.

I. INTRODUCTION

In the realm of ceramic materials for hard-coating applications, transition-metal diborides (MB_2) have garnered significant attention in recent years, in particular those crystallized in the hexagonal AlB_2 -type structure with the $P6/mmm$ space group [1–13]. The diborides stand out due not only to their high thermal and chemical stabilities, good mechanical properties, but also to the possibility of fine-tuning their properties through alloying. The adoption of alloying strategies to form double-metal diborides ($\text{M}'_x\text{M}''_{1-x}\text{B}_2$), as demonstrated through both theoretical and experimental investigations, has proven instrumental in substantially enhancing the stabilities and/or properties compared to their constituent diboride compounds ($\text{M}'\text{B}_2$ and $\text{M}''\text{B}_2$) [4–6, 8–13]. For example, the introduction of Al atoms into TiB_2 has been proven to enhance the oxidation and corrosion resistances of the material. Moreover, the mechanical properties of the resulting off-stoichiometric $\text{Ti}_{1-x}\text{Al}_x\text{B}_{2\pm\delta}$ can be improved or tailored by controlling its chemical composition, as reposted by Bakhit *et al* [8]. Another compelling instance is observed in the case of $\text{Sc}_x\text{Ta}_{1-x}\text{B}_2$ solid solutions, where first-principles calculations conducted by Mopoung *et al* [13] have recently revealed that a band-filling mechanism, modulated by the composition of the constituent compounds, plays a major role in determining and enhancing their stability and mechanical properties.

In addition, the substitution of vacancies for either M atoms or B atoms of MB_2 has been identified as a substantial factor influencing the stability and elastic properties of some metal diborides, for example, TaB_2 and NbB_2 , as elucidated by Dahlqvist *et al* [14]. The remarkable improvement of the stability, as well as the elastic properties of those diborides due to the participation of vacancies, can be attributed to the influence of electronic band filling. This seamlessly aligns with the theoretical findings of Ektarawong *et al* [15], who recently revised the binary Ta–B convex hull. The study not only confirmed the thermodynamic stability of $\text{TaB}_{2-\delta}$ where $0.167 \leq \delta \leq 0.25$ due to the presence of vacancies on the boron sublattice but also reported a significant enhancement in mechanical properties, especially hardness (with an approximate increase of 40%), of the material. It is worth noting that the values for different elastic quantities of B-deficient $\text{TaB}_{2-\delta}$, evaluated by Ektarawong *et al* [15] are quantitatively in good agreement with existing experimental data on the elastic properties of tantalum diboride [2, 16]. Furthermore, as demonstrated by Johansson *et al* [17], AlB_2 is not thermodynamically stable in stoichiometric form and exhibits a strong preference for Al vacancies to stabilize the material in the form of $\text{Al}_{1-\delta}\text{B}_2$, where $0.076 \leq \delta \leq 0.089$, and the vacancies are found to exert a notable influence on the electronic and vibrational properties of the material.

Among several double-metal diborides, having been suggested to be potential candidates for hard coating ap-

plications [5, 8, 10, 11, 13], $\text{Ta}_x\text{Al}_{1-x}\text{B}_2$ resulting from mixing TaB_2 with AlB_2 has barely been explored. Recently, Šroba *et al* [18] demonstrated through their experiments the insolubility of Al in TaB_2 , as observed in their magnetron co-sputtered $\text{Ta}_{0.75}\text{Al}_{0.25}\text{B}_{2.14}$ and $\text{Ta}_{0.69}\text{Al}_{0.31}\text{B}_{2.16}$ films. This, however, contradicts the theoretical predictions, derived from the density functional theory calculations, of Alling *et al* [5] that Ta and Al atoms in $\text{Ta}_x\text{Al}_{1-x}\text{B}_2$ display chemical ordering and it thus leads to the formation of an ordered solid solution of $\text{Ta}_{0.5}\text{Al}_{0.5}\text{B}_2$, thermodynamically stable up to at least 1273 K. Moreover, according to the theoretical and experimental studies of Šroba *et al* [18], introducing Al in TaB_2 seemingly results in decreases both of elastic moduli and the hardness of the material. Such contradiction between experimental observations and theoretical predictions in terms of the mixing thermodynamics of Ta and Al in $(\text{Ta,Al})\text{B}_2$ solid solutions raises several important but unanswered questions related to the stability and perhaps also the properties of $(\text{Ta,Al})\text{B}_2$, which are given as follows: (i) How does the addition of Al atoms into TaB_2 actually affect its thermodynamic stability as well as its electronic and elastic properties? (ii) Is there a possibility for vacancies to partially substitute for Ta, Al and/or B atoms in $(\text{Ta,Al})\text{B}_2$, as previously observed for TaB_2 [15] and AlB_2 [17]? (iii) If $(\text{Ta,Al})\text{B}_2$ shows a preference for the formation of vacancies, as stated in (ii), what are the stable chemical compositions and atomic configurations of the solid solutions under thermodynamic equilibrium conditions? (iv) How does the presence of vacancies in $(\text{Ta,Al})\text{B}_2$ affect its thermodynamic stability as well as its electronic and elastic properties? (v) Lastly, could the presence of vacancies in $(\text{Ta,Al})\text{B}_2$ be an explanation for the discrepancies between experimental observations and theoretical predictions in terms of the mixing behavior of Ta and Al in $(\text{Ta,Al})\text{B}_2$?

To provide answers to the above questions, we in this work conducted the density functional theory (DFT) calculations [19, 20], together with the cluster-expansion (CE) formalism [21, 22] to investigate the thermodynamic stability as well as the electronic and elastic properties of $(\text{Ta,Al})\text{B}_2$ solid solutions, and also to evaluate the impact of vacancy formation on the stability and the properties of the solid solutions. Our investigation unveils $(\text{Ta,Al})\text{B}_2$ solid solutions without the presence of vacancies are not thermodynamically stable. However, we showed that partial substitution of vacancies for Al atoms in $(\text{Ta,Al})\text{B}_2$ at some specific compositions can lead to thermodynamic stabilization of the materials. Furthermore, we reconstructed the convex hull for the ternary Ta–Al–B system, and demonstrated how the presence of vacancies affects the electronic and elastic properties of Al-deficient $(\text{Ta,Al})\text{B}_2$. Our findings and also detailed discussion on Al-deficient $(\text{Ta,Al})\text{B}_2$ are indeed essential for a more comprehensive understanding of the alloying behavior of $(\text{Ta,Al})\text{B}_2$. Such insights are of great impor-

tance for guiding future studies and the development of these ceramic materials.

II. COMPUTATIONAL DETAILS

A. First-principles calculations

We applied the enumeration algorithm [23], as implemented in the integrated cluster expansion toolkit (ICET) package [24] to the hexagonal primitive unit cell of AlB_2 -type TaB_2 ($P6/mmm$ space group) in order to create a set of structural models containing up to 36-atom of ordered solid solutions of $(\text{Ta,Al})\text{B}_2$ and Al-deficient $(\text{Ta,Al})\text{B}_2$ in primitive supercells. The Vienna *ab initio* simulation package (VASP) [25, 26] was implemented to perform all total-energy calculations, based on the density functional theory (DFT) [19, 20]. This employed the projector augmented wave (PAW) method [27, 28], together with the generalized gradient approximation (GGA) [29] for description of the electronic exchange-correlation effects. In this work, the plane-wave energy cut-off was set to 500 eV and the Monkhorst-Pack k-point grids [30] was used for the integration of the Brillouin zone. Also, we ensured the numerical convergence of the calculated total energy within 1 meV/atom with respect to the plane-wave energy cut-off and the number of k-point grids. To minimize the total energy (E_{tot}) of all $(\text{Ta,Al})\text{B}_2$ and Al-deficient $(\text{Ta,Al})\text{B}_2$, their structural models were allowed to fully relax during the DFT calculations. For the total electronic density of states (DOS) calculations, the Monkhorst-Pack k-point sampling was used together with the tetrahedron method [31].

B. Cluster-expansion formalism

To identify the ground-state configurations of either $(\text{Ta,Al})\text{B}_2$ or Al-deficient $(\text{Ta,Al})\text{B}_2$ due to the presence of vacancies, we utilized the cluster-expansion method [21, 22] for the expansion of their mixing energies $\Delta E_{mix}(\boldsymbol{\sigma})$. According to this approach, the $\Delta E_{mix}(\boldsymbol{\sigma})$ of any atomic configuration $\boldsymbol{\sigma}$ of the alloy system under consideration can be expanded as:

$$\Delta E_{mix}(\boldsymbol{\sigma}) = \sum_{\alpha} m_{\alpha} J_{\alpha} \Gamma_{\alpha}(\boldsymbol{\sigma}). \quad (1)$$

$\Gamma_{\alpha}(\boldsymbol{\sigma})$ represents the cluster correlation function of a symmetry-equivalent cluster α . The m_{α} and J_{α} parameters are the multiplicity and the effective cluster interactions (ECIs) of cluster α , respectively, corresponding to the $\Gamma_{\alpha}(\boldsymbol{\sigma})$. Here, a set of $\Gamma_{\alpha}(\boldsymbol{\sigma})$ called correlation vectors was used to represent unique ordered configurations of $(\text{Ta,Al})\text{B}_2$ and Al-deficient $(\text{Ta,Al})\text{B}_2$. Each $\Gamma_{\alpha}(\boldsymbol{\sigma})$ is defined through the product of spin designations of

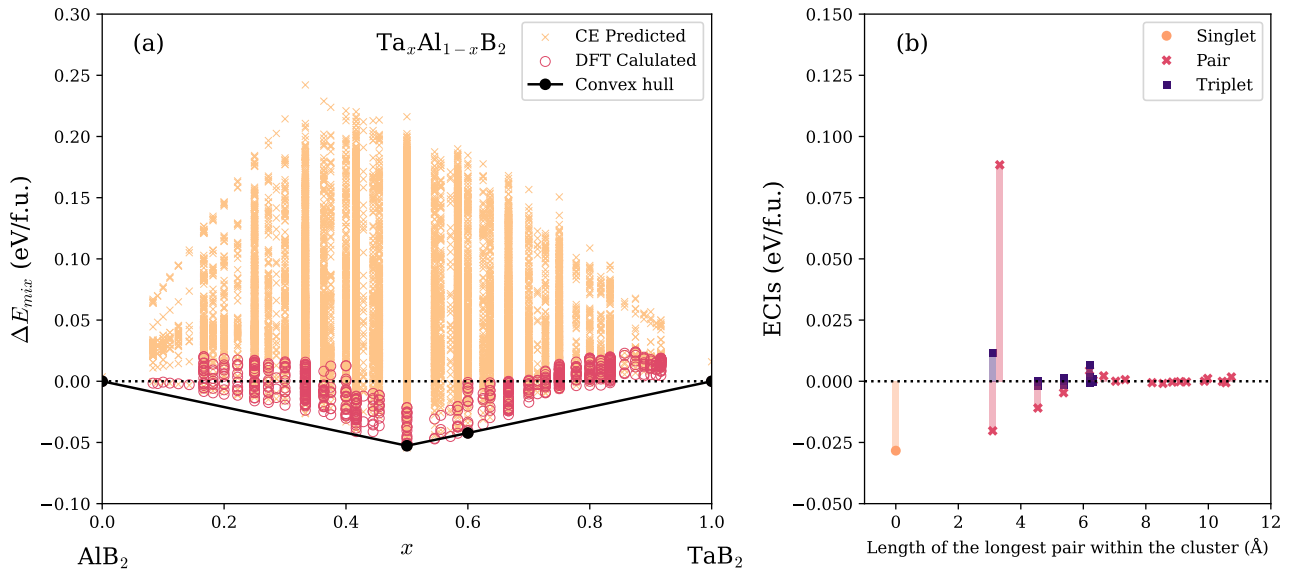


FIG. 1: (a) Mixing energies of $Ta_xAl_{1-x}B_2$ (ΔE_{mix}), where $0 \leq x \leq 1$, calculated within up-to-36 atom primitive supercells. The orange crosses represent CE-predicted ΔE_{mix} of 20,421 enumerated configurations of $Ta_xAl_{1-x}B_2$, whereas the red hollow circles represent DFT-calculated ΔE_{mix} of 742 configurations of $Ta_xAl_{1-x}B_2$, used in the final fitting process. The black-filled circles with connected lines at $x = 0, 0.5, 0.6$, and 1 , represent the convex hull of $Ta_xAl_{1-x}B_2$. (b) Strength of 32 effective cluster interactions (ECIs) between Ta and/or Al atoms residing on the metal sublattice of $Ta_xAl_{1-x}B_2$, obtained from the cluster expansion. The ECIs consist of 1 singlet (yellow circle), 19 pairs (red crosses), and 12 triplets (purple squares).

atoms and/or vacancies participating in the alloying process. For the pseudo-binary solid solutions $(Ta,Al)B_2$, the CE formalism for regular binary alloys, as described in our previous works, was directly used [15, 32]. However, for Al-deficient $(Ta,Al)B_2$, we employed the multi-components CE formalism [33–35], considering the atomic configuration of Ta and Al atoms, as well as vacancies within the metal sublattice of $(Ta,Al)B_2$.

Through the implementation of the ICET package, we determine two different conditions for the construction of correlation vectors. The first condition is for the correlation vectors of $(Ta,Al)B_2$, comprising a singlet, 19 pairs, and 12 triplets, while the other condition comprising of 2 singlets, 39 pairs, and 58 triplets is for the correlation vectors of Al-deficient $(Ta,Al)B_2$. The process of fitting the ECIs was conducted utilizing LASSO regression via scikit-learn package [36] based on the reference data obtained from the DFT calculations to predict $\Delta E_{mix}(\sigma)$ for all enumerated configurations both of $(Ta,Al)B_2$ and Al-deficient $(Ta,Al)B_2$.

C. Elastic properties calculations

To obtain the elastic properties of these structures, the elastic constants C_{ij} of $(Ta,Al)B_2$ and Al-deficient $(Ta,Al)B_2$ of a given configuration σ were evaluated using the second derivative of the total energy $E_{tot}(\epsilon)$ with

respect to strain ϵ_i , defined as:

$$C_{ij} = \frac{1}{V_{eq}} \left. \frac{\partial^2 E_{tot}(\epsilon)}{\partial \epsilon_i \partial \epsilon_j} \right|_{\epsilon=0}. \quad (2)$$

For this particular case, $E_{tot}(\epsilon)$ is expanded into a power series of the strain vector ϵ in Voigt's notation, $\epsilon = (\epsilon_{xx}, \epsilon_{yy}, \epsilon_{zz}, 2\epsilon_{xy}, 2\epsilon_{xz}, 2\epsilon_{yz}) \equiv (\epsilon_1, \epsilon_2, \epsilon_3, \epsilon_4, \epsilon_5, \epsilon_6)$, where ϵ_i represents the strain along the i -th direction and V_{eq} is the equilibrium volume of σ of $(Ta,Al)B_2$ or Al-deficient $(Ta,Al)B_2$ under consideration [37]. Regarding the practical implementation, $E_{tot}(\epsilon)$ was obtained by applying strains ϵ_i of $\pm 1\%$ and $\pm 2\%$ distortions without volume conservation to the fully relaxed structure and then relaxing the atomic coordinates within the structure. The lattice vectors were fixed during this relaxation step. The energies at different degrees of distortion were evaluated through DFT calculations and then fitted to a quadratic function.

For interpreting the elastic constants of the hexagonal system, the C_{ij} from Eq.2 were projected onto six projected hexagonal elastic constants \bar{C}_{ij} , including \bar{C}_{11} , \bar{C}_{12} , \bar{C}_{13} , \bar{C}_{33} , \bar{C}_{44} , and \bar{C}_{66} using a symmetry-based projection method [15, 38]. The \bar{C}_{ij} for all structures were examined to satisfy the necessary conditions for mechanical stability in the hexagonal system [39]. The projec-

tions and the conditions are defined as follows:

$$\begin{aligned}\bar{C}_{11} &= \frac{3}{8}(C_{11} + C_{22}) + \frac{1}{4}C_{12} + \frac{1}{2}C_{66}, \\ \bar{C}_{12} &= \frac{1}{8}(C_{11} + C_{22}) + \frac{1}{4}C_{12} - \frac{1}{2}C_{66}, \\ \bar{C}_{13} &= \frac{1}{2}(C_{13} + C_{23}), \quad \bar{C}_{33} = C_{33}, \\ \bar{C}_{44} &= \frac{1}{2}(C_{44} + C_{55}), \quad \bar{C}_{66} = \frac{1}{2}(\bar{C}_{11} - \bar{C}_{12}).\end{aligned}\tag{3a}$$

$$\text{conditions: } \begin{cases} \bar{C}_{11} > |\bar{C}_{12}|, \\ \bar{C}_{33}(\bar{C}_{11} + \bar{C}_{12}) > 2\bar{C}_{13}^2, \\ \bar{C}_{44} > 0, \bar{C}_{66} > 0 \end{cases}\tag{3b}$$

These \bar{C}_{ij} provide the interpretable description of the elastic behavior using the Voigt-Reuss-Hill method [40] to calculate the bulk modulus (B), shear modulus (G), and Young's modulus (E), that indicate the resistance of our structures to bulk compression, shear stress, and normal stress, respectively. Other mechanical properties like Vickers hardness (H) and the bulk-to-shear ratio (B/G) were also estimated in this work. The hardness represents the resistance to localized plastic deformation of materials. For this work, we estimated H from correlations with G and B moduli, following the semi-empirical model developed by Chen *et al* [41], which have been shown to agree well with experimental values for AlB₂-type MB₂, particularly AlB₂-type TaB₂ [42]. According to the model, hardness can be expressed as:

$$H = 2\left(\frac{G^3}{B^2}\right)^{0.585} - 3.\tag{4}$$

Furthermore, the B/G ratio can be used to indicate the brittleness or ductility of materials. According to Pugh's criteria [43], any materials with the B/G ratio values larger than the critical value of 1.75 are distinguished to be ductile materials, whereas those with the B/G ratio values lower than the critical value are all brittle.

III. RESULTS AND DISCUSSION

A. Pseudo-binary convex hull of (Ta,Al)B₂

Previously, Johansson *et al* demonstrated the thermodynamic stability of Al-deficient Al_{1- δ} B₂ within the narrow range of $0.076 \leq \delta \leq 0.089$ due to the presence of Al vacancies [17], and Ektarawong *et al* revealed the thermodynamic stability of B-deficient TaB_{2- δ} within the range of $0.167 \leq \delta \leq 0.25$ due to the presence of vacancies on the boron sublattice [15]. The preliminary step of this

work, however, begins with the examination of thermodynamic stability within the pseudo-binary (Ta,Al)B₂ system without any vacancies. Fig. 1(a) displays $\Delta E_{mix}(\sigma)$ of Ta _{x} Al_{1- x} B₂, where $0 \leq x \leq 1$, evaluated with respect to TaB₂ and AlB₂, and defined as:

$$\Delta E_{mix}(\sigma) = E_{tot}(\sigma) - xE_{tot}(\text{TaB}_2) - (1-x)E_{tot}(\text{AlB}_2),\tag{5}$$

where σ in Eq. 5 represents any unique configuration of Ta _{x} Al_{1- x} B₂. In the present work, the DFT-derived $\Delta E_{mix}(\sigma)$ of 742 distinct configurations of Ta _{x} Al_{1- x} B₂ (the red hollow circles in Fig. 1(a)) were employed as reference data for the fitting process, which was conducted through the use of the CE method outlined in II B with the resulting cross-validation score of 6 meV/f.u. This ensures the predictive capability of the fitting procedure. Subsequently, the determined ECIs were utilized to predict the $\Delta E_{mix}(\sigma)$ of the remaining enumerated σ of ordered Ta _{x} Al_{1- x} B₂ as represented by the orange crosses in Fig. 1(a).

The manifestation of negative values of $\Delta E_{mix}(\sigma)$ for numerous configurations σ of Ta _{x} Al_{1- x} B₂ indicates a tendency of mixing between TaB₂ and AlB₂, where Ta _{x} Al_{1- x} B₂ display chemical ordering of Ta and Al atoms, as the temperature approaches absolute zero. These results align qualitatively with the theoretical predictions, previously reported by Alling *et al* [5] and Šroba *et al* [18]. In addition, the atomic configuration σ plays a main factor influencing $\Delta E_{mix}(\sigma)$ within this system, as can be seen in Fig. 1(a). Our findings, illustrated in Fig. 1(b), highlight the significant impact of ECIs between Ta and Al atoms in this system. Particularly, it should be noted that the predominant interaction is the pair interaction corresponding to the second coordination shell (shortest interlayer bond distance between Ta and/or Al atoms) with a positive value of 0.09 eV/f.u., followed by the singlet interaction of -0.03 eV/f.u. governed by the relative content of Ta and Al, and the pair interaction corresponding to the first coordination shell (shortest intralayer bond distance between Ta and/or Al atoms) of -0.02 eV/f.u., respectively. Apart from these 3 ECIs, the strengths of other ECIs, whose magnitudes are lower than 0.02 eV/f.u., are less significant.

Among all the configurations of Ta _{x} Al_{1- x} B₂ presented in Fig. 1(a), $\Delta E_{mix}(\sigma)$ of TaB₂, AlB₂, two ordered solid solutions of Ta _{x} Al_{1- x} B₂ with $x = 0.5$ and 0.6 lie on the convex hull of the pseudo-binary TaB₂-AlB₂ system (four black-filled circles connected by the thick black line), suggesting that they are candidates for ground-state configurations of Ta _{x} Al_{1- x} B₂. The visualization of these four candidates is displayed in Fig. S1. Our ground-state configurations of Ta_{0.5}Al_{0.5}B₂ and Ta_{0.6}Al_{0.4}B₂ show the $\Delta E_{mix}(\sigma)$ of approximately -0.05 eV/f.u. and -0.04 eV/f.u., respectively, which are lower than that of the ordered solid solution of Ta_{0.5}Al_{0.5}B₂ reported in

TABLE I: Formation energies of vacancy (ΔE_{vac}) for all inequivalent crystallographic sites of Ta, Al, and B in the dilute limit of $\text{Ta}_{0.5}\text{Al}_{0.5}\text{B}_2$ and $\text{Ta}_{0.6}\text{Al}_{0.4}\text{B}_2$. Type of vacancy ($V_{A(i)}$) denotes an inequivalent crystallographic site i of atom A where A = Al, Ta, or B, replaced by a vacancy (see also their visualizations in Fig. S2). The ΔE_{vac} is evaluated by Eq. 6 where a single atom of A is removed from the ideally defect-free solid solutions, which are modeled within sufficiently large supercells.

Composition	Supercell size (Number of atoms)	Type of vacancy	ΔE_{vac} (eV/vacancy)
$\text{Ta}_{0.5}\text{Al}_{0.5}\text{B}_2$	$3 \times 3 \times 2$ (648 atoms)	$V_{\text{Al}(1)}$	-0.769
		$V_{\text{Al}(2)}$	-0.934
		$V_{\text{Al}(3)}$	-0.855
		$V_{\text{Ta}(1)}$	1.591
		$V_{\text{Ta}(2)}$	1.381
		$V_{\text{Ta}(3)}$	1.629
$\text{Ta}_{0.6}\text{Al}_{0.4}\text{B}_2$	$3 \times 3 \times 2$ (540 atoms)	$V_{\text{B}(1)}$	1.093
		$V_{\text{Al}(1)}$	-0.941
		$V_{\text{Al}(2)}$	-0.970
		$V_{\text{Ta}(1)}$	0.953
		$V_{\text{Ta}(2)}$	1.449
		$V_{\text{Ta}(3)}$	1.331
		$V_{\text{B}(1)}$	0.872
		$V_{\text{B}(2)}$	0.734

Ref. [18] by around 0.01 eV/f.u. It is worth further noting that $\Delta E_{mix}(\boldsymbol{\sigma})$ of our ground-state $\text{Ta}_{0.5}\text{Al}_{0.5}\text{B}_2$ and $\text{Ta}_{0.6}\text{Al}_{0.4}\text{B}_2$ are still significantly lower than the mean-field estimated mixing Gibbs free energy (ΔG_{mix}) at 1473 K of random solid solutions of $\text{Ta}_x\text{Al}_{1-x}\text{B}_2$, where $0 \leq x \leq 1$, as reported also in Ref. [18]. This suggests chemical ordering of Ta and Al atoms in $\text{Ta}_x\text{Al}_{1-x}\text{B}_2$ solid solutions is retained up to at least ~ 1500 K. In addition, it should be noted here that the convex hull of this pseudo-binary (Ta,Al) B_2 system, constructed from the DFT calculations, concurs with that predicted by the CE approach.

B. Formation of vacancies in (Ta,Al) B_2

To investigate whether Ta, Al or B atoms in (Ta,Al) B_2 solid solutions can partially be substituted by vacancies, as previously observed in their constituent compounds, we firstly examined the formation of vacancies at each site of an atom within the dilute limit of our ground-state configurations of (Ta,Al) B_2 . The formation of vacancies in the dilute limit is characterized by the defect formation energy (ΔE_{vac}), delineated as:

$$\Delta E_{vac} = E_{vac} - (E_{vac-free} - \sum_A \mu_A N_A). \quad (6)$$

Here, E_{vac} ($E_{vac-free}$) stands for the total energy of the defective (defect-free) (Ta,Al) B_2 , modeled within a supercell, containing at least 540 atoms. The summation in Eq. 6 encompasses all relevant atomic species (A = Al, Ta, and B), where μ_A represents the chemical potential of A atom, and N_A denotes the number of removed A atoms from the supercell. In this case, the defective struc-

tures of ordered $\text{Ta}_{0.5}\text{Al}_{0.5}\text{B}_2$ and ordered $\text{Ta}_{0.6}\text{Al}_{0.4}\text{B}_2$ are constructed by selectively removing only a single Al, Ta, or B atom from the supercell for all of its possible inequivalent crystallographic sites, and the chemical potentials μ_{Al} , μ_{Ta} , and μ_{B} are estimated from the total energies per atom of face-centered cubic Al, body-centered cubic Ta, and α -rhombohedral B, respectively.

The calculated values of ΔE_{vac} for ordered solid solutions of $\text{Ta}_{0.5}\text{Al}_{0.5}\text{B}_2$ and $\text{Ta}_{0.6}\text{Al}_{0.4}\text{B}_2$ are listed in Table I. Our findings reveal that only ΔE_{vac} for Al vacancies in the dilute limit of both $\text{Ta}_{0.5}\text{Al}_{0.5}\text{B}_2$ and $\text{Ta}_{0.6}\text{Al}_{0.4}\text{B}_2$ exhibit negative values, with a magnitude of ~ 1 eV/vacancy across all sites. Conversely, the values of ΔE_{vac} for Ta and B vacancies are all positive. The negative values of ΔE_{vac} observed for Al vacancies in these structures suggest an improvement in the solutions' stability. That is, the solid solutions with reduced Al content could be more favorable from the thermodynamic point of view, and it indicates the substantial contribution of Al vacancies, which from now on will be denoted as Va with vacancy concentration of μ , to the thermodynamic stability of $\text{Ta}_{0.5}\text{Al}_{0.5}\text{B}_2$ and $\text{Ta}_{0.6}\text{Al}_{0.4}\text{B}_2$.

To search for candidates for ground-state configurations of Al-deficient (Ta,Al) B_2 due to the presence of Al vacancies, based on the two ground-states structures of $\text{Ta}_{0.5}\text{Al}_{0.5}\text{B}_2$ and $\text{Ta}_{0.6}\text{Al}_{0.4}\text{B}_2$, we generated structural models containing up to 36-atom of Al-deficient (Ta,Al) B_2 in primitive supercells, where Ta, Al, and Va are uniquely distributed in the ordered manner on the metal sublattice of the solid solutions. For fixed Ta contents with $x = 0.5$ and 0.6 of $\text{Ta}_x\text{Al}_{1-x}\text{B}_2$, we reduced Al content from the two ground-state structures to model $\text{Ta}_{0.5}\text{Al}_{0.5-\mu}\text{Va}_\mu\text{B}_2$ and $\text{Ta}_{0.6}\text{Al}_{0.4-\mu}\text{Va}_\mu\text{B}_2$ with $0 < \mu \leq 0.167$. By performing the DFT calculations in combi-

nation with the CE method, Figs. 2(a) and 2(b) illustrate, respectively, mixing energies of $\text{Ta}_{0.5}\text{Al}_{0.5-\mu}\text{Va}_{\mu}\text{B}_2$ ($\Delta E'_{mix}(\boldsymbol{\sigma})$) and $\text{Ta}_{0.6}\text{Al}_{0.4-\mu}\text{Va}_{\mu}\text{B}_2$ ($\Delta E''_{mix}(\boldsymbol{\sigma})$) where $0 < \mu \leq 0.167$. The $\Delta E'_{mix}(\boldsymbol{\sigma})$ is defined as the mixing energies of $\text{Ta}_{0.5}\text{Al}_{0.5-\mu}\text{Va}_{\mu}\text{B}_2$ assessed in relation to the lowest-energy configurations of $\text{Ta}_{0.5}\text{Al}_{0.5}\text{B}_2$ ($\boldsymbol{\sigma}_{\mu=0}^{GS}$) and $\text{Ta}_{0.5}\text{Al}_{0.333}\text{Va}_{0.167}\text{B}_2$ ($\boldsymbol{\sigma}_{\mu=0.167}^{GS}$), identified in this work and expressed as:

$$\Delta E'_{mix}(\boldsymbol{\sigma}) = E_{tot}(\boldsymbol{\sigma}) - \frac{\mu}{0.167}E_{tot}(\boldsymbol{\sigma}_{\mu=0.167}^{GS}) - (1 - \frac{\mu}{0.167})E_{tot}(\boldsymbol{\sigma}_{\mu=0}^{GS}), \quad (7)$$

where $\boldsymbol{\sigma}$ denotes any configuration of $\text{Ta}_{0.5}\text{Al}_{0.5-\mu}\text{Va}_{\mu}\text{B}_2$ with $\mu = 0, 0.083, 0.1, 0.125, 0.167$.

On the other hand, $\Delta E''_{mix}(\boldsymbol{\sigma})$ is defined as the difference in energy of $\text{Ta}_{0.6}\text{Al}_{0.4-\mu}\text{Va}_{\mu}\text{B}_2$ relative to the lowest-energy configuration of $\text{Ta}_{0.6}\text{Al}_{0.4-\mu}\text{Va}_{\mu}\text{B}_2$ with

$\mu = 0.1$ ($\boldsymbol{\sigma}_{\mu=0.1}^{GS}$) found in the present work, and it can be expressed as:

$$\Delta E''_{mix}(\boldsymbol{\sigma}) = E_{tot}(\boldsymbol{\sigma}) - E_{tot}(\boldsymbol{\sigma}_{\mu=0.1}^{GS}). \quad (8)$$

Also, $\boldsymbol{\sigma}$ signifies any configuration of $\text{Ta}_{0.6}\text{Al}_{0.3}\text{Va}_{0.1}\text{B}_2$. Following the previously outlined CE procedure, the final sets of ECIs were determined by fitting the $\Delta E'_{mix}(\boldsymbol{\sigma})$ ($\Delta E''_{mix}(\boldsymbol{\sigma})$) of unique 1,253 (391) training configurations with the cross-validation score of 0.078 (0.015) eV/f.u. for $\text{Ta}_{0.5}\text{Al}_{0.5-\mu}\text{Va}_{\mu}\text{B}_2$ where $0 < \mu \leq 0.167$ ($\text{Ta}_{0.6}\text{Al}_{0.3}\text{Va}_{0.1}\text{B}_2$) to identify its ground-state candidates, as all represented in Fig. 2 by the red hollow circles. The mixing energies for the remaining configurations of Al-deficient $(\text{Ta},\text{Al})\text{B}_2$, predicted from the CE models, are also depicted in Fig. 2 (the orange crosses). The mixing energies for the remaining configurations of Al-deficient $(\text{Ta},\text{Al})\text{B}_2$, predicted from the CE models, are also depicted in Fig. 2 (the orange crosses). Fig. 2 also shows the convex hull construction of these two cases — the singular ground-state configuration of $\text{Ta}_{0.6}\text{Al}_{0.3}\text{Va}_{0.1}\text{B}_2$ and the $\text{Ta}_{0.5}(\text{Al},\text{Va})\text{B}_2$ convex hull — by the thick black lines connecting the black-filled circles. This overall presents three Al-deficient $(\text{Ta},\text{Al})\text{B}_2$ configurations as novel ground-state candidates for the Ta–Al–B system with compositions of $\text{Ta}_{0.6}\text{Al}_{0.3}\text{Va}_{0.1}\text{B}_2$, $\text{Ta}_{0.5}\text{Al}_{0.417}\text{Va}_{0.083}\text{B}_2$, and $\text{Ta}_{0.5}\text{Al}_{0.333}\text{Va}_{0.167}\text{B}_2$, as depicted in Fig. S3.

C. Construction of ternary ground-state diagram for Ta–Al–B system

To sketch the ternary ground-state diagram of the Ta–Al–B system and to visualize the thermodynamic stability both of $(\text{Ta},\text{Al})\text{B}_2$ and of Al-deficient $(\text{Ta},\text{Al})\text{B}_2$, we evaluated the stability of our identified ground-state candidates with respect to all relevant competing phases in the Ta–Al–B system. Those are Ta_3B_2 , TaB , Ta_5B_6 , Ta_3B_4 , Ta_2Al , $\text{Ta}_{48}\text{Al}_{38}$, TaAl_3 , face-centered cubic Al, body-centered cubic Ta, and α -rhombohedral B. Herein, we considered also ground-state configurations of Al-deficient $\text{Al}_{1-\delta}\text{B}_2$ and B-deficient $\text{TaB}_{2-\delta}$, which were predicted in Refs. [15, 17] to be thermodynamically stable even at absolute zero. These configurations were included as competing phases for $(\text{Ta},\text{Al})\text{B}_2$ and Al-deficient $(\text{Ta},\text{Al})\text{B}_2$. It is important to note that TaB_2 was considered in many different prototypes of MB_2 structures, all of which lie above the Ta–B convex hull because of including AlB_2 -type $\text{TaB}_{2-\delta}$ in our consideration. On the other hand, the presence of both Ta and B vacancies as well as other types of structural point defects does not qualitatively improve phase stability in other prototypes, as revealed in Ref. [15]. Formation energies (E_f) of all structures were computed in terms of total energies per atom evaluated concerning three pure phases, face-centered cubic Al, body-centered cubic Ta, and α -rhombohedral B. Subsequently, the Ta–Al–B convex hull was constructed in three dimensions and mapped onto the two-dimensional ternary ground-state

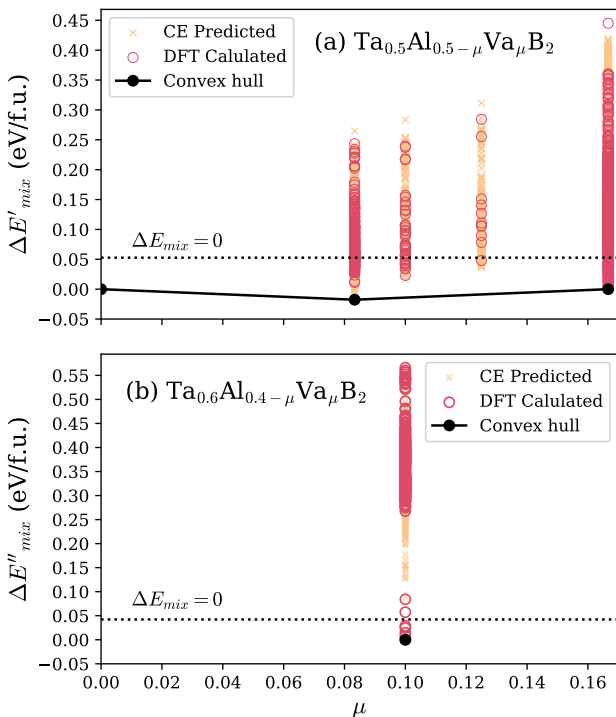


FIG. 2: (a) Mixing energies of $\text{Ta}_{0.5}\text{Al}_{0.5-\mu}\text{Va}_{\mu}\text{B}_2$ ($\Delta E'_{mix}$), calculated within up-to-36 atom primitive supercells, and (b) mixing energies of $\text{Ta}_{0.6}\text{Al}_{0.4-\mu}\text{Va}_{\mu}\text{B}_2$ ($\Delta E''_{mix}$), modeled within 30-atom primitive supercells, where $0 < \mu \leq 0.167$. The orange crosses represent CE-predicted mixing energies of enumerated configurations, whereas the red hollow circles represent DFT-calculated mixing energies. The black-filled circles with connected lines in (a) at $\mu = 0, 0.083$ and 0.167 , represent the convex hull of $\text{Ta}_{0.5}\text{Al}_{0.5-\mu}\text{Va}_{\mu}\text{B}_2$ and the black-filled circle in (b) at $\mu = 0.1$ is the lowest $\Delta E''_{mix}$ among the considered configurations of $\text{Ta}_{0.6}\text{Al}_{0.3}\text{Va}_{0.1}\text{B}_2$. The black dashed lines indicate the values of $\Delta E'_{mix}$ or $\Delta E''_{mix}$ that are equal to 0 eV/f.u. of ΔE_{mix} , mixing energies of vacancy-free $\text{Ta}_x\text{Al}_{1-x}\text{B}_2$, in Fig 1(a).

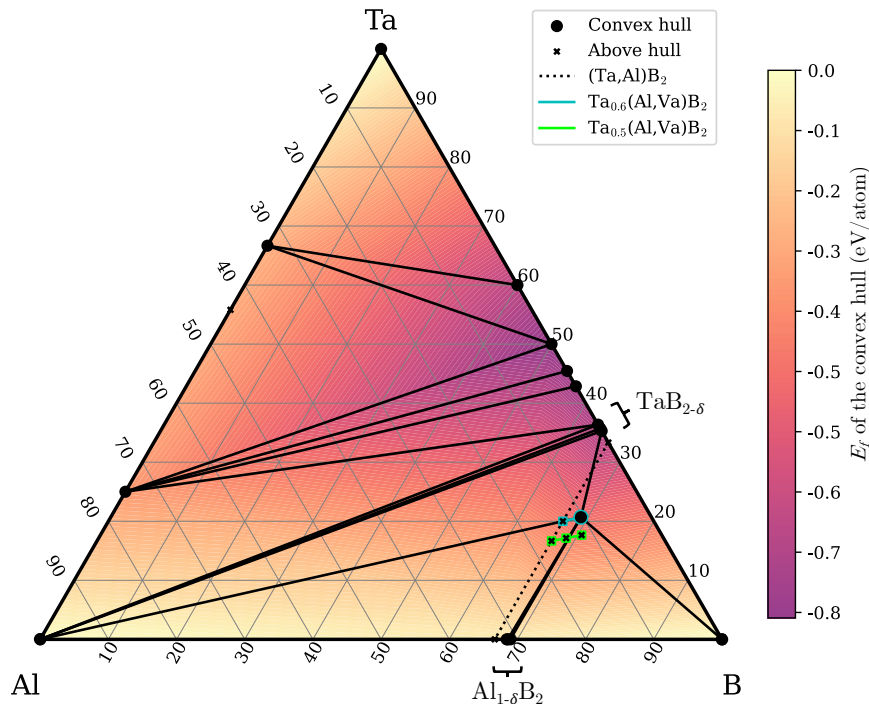


FIG. 3: Ternary diagram visualizing the thermodynamic stability of $(\text{Ta},\text{Al})\text{B}_2$, Al-deficient $(\text{Ta},\text{Al})\text{B}_2$, and all relevant competing phases at absolute zero in Ta–Al–B system. The contour colormap represents the formation energy (E_f) of the convex hull in eV/atom. The black circles denote the phases lying on the convex hull, and the black crosses denote the phases lying above the convex hull. The pseudo-binary alloys of $(\text{Ta},\text{Al})\text{B}_2$, $\text{Ta}_{0.5}(\text{Al},\text{Va})\text{B}_2$, and $\text{Ta}_{0.6}(\text{Al},\text{Va})\text{B}_2$ are represented by the black dotted line, the blue line, and the green line, respectively.

diagram, as illustrated in Fig. 3. Additionally, the E_f and energies above the convex hull of all considered prototypes of TaB_2 structures are listed in Table S1.

The diagram reveals that AlB_2 and TaB_2 persistently lie above our sketched Ta–Al–B convex hull, consistent with previous results in both the Al–B convex hull [17] and the Ta–B convex hull [15]. Furthermore, the solid solutions of $\text{Ta}_x\text{Al}_{1-x}\text{B}_2$ lying along the straight line drawn between TaB_2 and AlB_2 (the black dotted line in Fig. 3) were verified to be positioned above our constructed convex hull. According to our predictions, the E_f of ground-state $\text{Ta}_{0.5}\text{Al}_{0.5}\text{B}_2$ and $\text{Ta}_{0.6}\text{Al}_{0.4}\text{B}_2$ are, respectively, 14 meV/atom and 22 meV/atom above the convex hull. These findings clearly underscore the instability of $\text{Ta}_x\text{Al}_{1-x}\text{B}_2$ solid solutions, and they are expected to undergo phase separation even at absolute zero into mixtures of more thermodynamically stable phases.

For the ground-state candidates of Al-deficient $(\text{Ta},\text{Al})\text{B}_2$, we present a visual representation of these candidates on the blue and green lines, separating from the black dotted line of $(\text{Ta},\text{Al})\text{B}_2$ shown in Fig. 3. As can be seen from Fig. 3, $\text{Ta}_{0.5}\text{Al}_{0.5-\mu}\text{Va}_\mu\text{B}_2$ where $\mu = 0.083$ and 0.167 lie above the hull, indicating also their instability. However, their E_f are merely slightly above the hull by less than 10 meV/atom. Interestingly, the $\text{Ta}_{0.6}\text{Al}_{0.3}\text{Va}_{0.1}\text{B}_2$ is positioned on the Ta–Al–B con-

vex hull, emerging as the sole thermodynamically stable configuration of the Al-deficient $(\text{Ta},\text{Al})\text{B}_2$ solid solutions considered in this work. This outcome indicates the potential stability of Al-deficient $(\text{Ta},\text{Al})\text{B}_2$ where the B/(Ta+Al) ratio is slightly over-stoichiometric, and the Ta content is roughly twice that of Al. Based on our proposed ternary diagram, one would expect that the solid solutions of $\text{Ta}_x\text{Al}_{1-x}\text{B}_2$ with $0.6 \leq x < 1$ may in thermodynamic equilibrium undergo phase separation into face-centered cubic Al, Al-deficient $\text{Ta}_{0.6}\text{Al}_{0.3}\text{Va}_{0.1}\text{B}_2$, and B-deficient $\text{TaB}_{2-\delta}$. This is seemingly in line with the experimental findings that $\text{Ta}_{0.75}\text{Al}_{0.25}\text{B}_{2.14}$ and $\text{Ta}_{0.69}\text{Al}_{0.31}\text{B}_{2.16}$ films were characterized to mainly be $\text{TaB}_{\sim 2}$ surrounded by the amorphous Al-rich regions [18]. However, it is essential to note that this suggestion was drawn only from the theoretical aspect, whereas the occurrence of an off-stoichiometric ratio and phase separation in as-synthesized materials can be influenced by various experimental factors.

D. Structural and electronic properties of Al-deficient $(\text{Ta},\text{Al})\text{B}_2$

We found that, in addition to the thermodynamic stability, the presence of vacancies essentially influences the

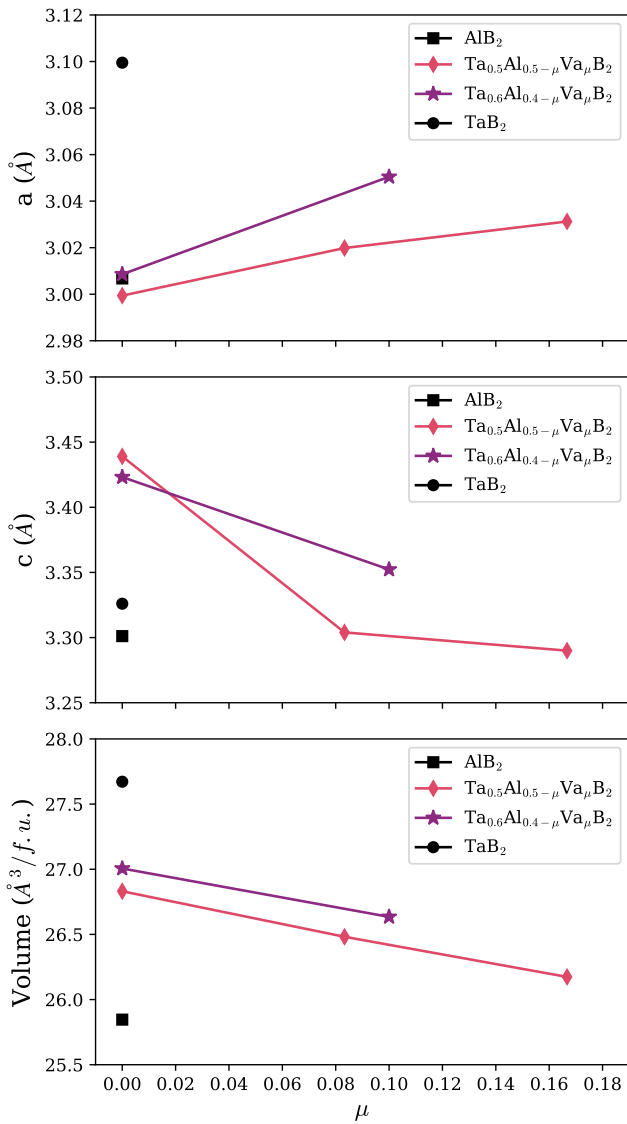


FIG. 4: Calculated lattice parameters (a and c) and unit-cell volume of AlB_2 (black square), $\text{Ta}_{0.5}\text{Al}_{0.5-\mu}\text{Va}_\mu\text{B}_2$ with $\mu = 0, 0.083, 0.167$ (red diamonds), $\text{Ta}_{0.6}\text{Al}_{0.4-\mu}\text{Va}_\mu\text{B}_2$ with $\mu = 0.1$ (purple stars), and TaB_2 (black circle), respectively.

structural and electronic properties of $(\text{Ta,Al})\text{B}_2$. Fig. 4 displays the DFT-calculated lattice parameters (a and c) and the unit-cell volume of the three ground-state structures of Al-deficient $(\text{Ta,Al})\text{B}_2$ in a comparison to their corresponding vacancy-free structures, AlB_2 , and TaB_2 . Notably, the lattice parameters of the two mono-metal diborides are closely in line with the values reported in the previous studies [3, 7, 14–18, 44, 45]. The changes in the lattice parameters for $\text{Ta}_x\text{Al}_{1-x}\text{B}_2$ with $x = 0.5$ (0.6) show that the parameter a falls roughly 3.2% (2.9%) from the parameter of TaB_2 (nearly the same as that of AlB_2), whereas its parameter c increases by around 3.4% (2.9%) with respect to that of TaB_2 . Additionally, the unit-cell volumes of the $\text{Ta}_x\text{Al}_{1-x}\text{B}_2$ solid solutions demonstrate

a linear trend drawn between the volumes of TaB_2 and AlB_2 , following Vegard’s law. These changes are in good agreement with the theoretical results of the $(\text{Ta,Al})\text{B}_2$ random solid solutions reported in [18]. The introduction of Al vacancies in $(\text{Ta,Al})\text{B}_2$ obviously alters the lattice parameters and the unit-cell volume of the solutions as compared to their corresponding vacancy-free structures. For $\text{Ta}_{0.5}\text{Al}_{0.417}\text{Va}_{0.083}\text{B}_2$, $\text{Ta}_{0.5}\text{Al}_{0.333}\text{Va}_{0.167}\text{B}_2$, and $\text{Ta}_{0.6}\text{Al}_{0.3}\text{Va}_{0.1}\text{B}_2$, the parameter a (c) are increased (decreased), respectively, by 0.7% (3.9%), 1.1% (4.3%), and 1.4% (2.1%), relative to that of their vacancy-free structures. This thus results in a linear reduction in the unit-cell volume of 1.3%, 2.4%, and 1.4%, respectively, compared to that of their vacancy-free structures.

The impact of Al vacancies on the electronic properties can be examined by analyzing changes in electronic density of states (DOS) of the solid solutions, as depicted in Fig. 5. The black lines in Figs. 5(a) - 5(d) represent the DOS of $\text{Ta}_x\text{Al}_{1-x}\text{B}_2$, where x takes on the values of 0, 0.5, 0.6, and 1, respectively, revealing metallic behavior of the materials with non-zero electronic states at the Fermi level. According to the bonding analysis of transition-metal diborides, crystallizing in the AlB_2 -type structure [5, 13, 14], a valley, observed below the Fermi level, also known as a pseudogap, typically separates the bonding states from the antibonding states due mainly to the interactions between atoms residing on the metal sublattice, and the stability of these diborides can to a large extent be influenced by occupation of electrons in these states [5]. In the case of $\text{Ta}_x\text{Al}_{1-x}\text{B}_2$, the pseudogap of $\text{Ta}_{0.5}\text{Al}_{0.5}\text{B}_2$ and $\text{Ta}_{0.6}\text{Al}_{0.4}\text{B}_2$ shifts toward the Fermi level relative to those of TaB_2 , because of the difference in the number of valence electrons between aluminum’s three valence electrons, compared to tantalum’s five valence electrons, as straightforwardly elucidated by Šroba *et al* [18]. This results in a decrease in the number of valence electrons occupying the antibonding states, as Al substitutes Ta atoms. Consequently, $\text{Ta}_x\text{Al}_{1-x}\text{B}_2$ demonstrates increased stability at the optimal compositions around x of 0.5 and 0.6, consistent with the observed ΔE_{mix} depicted in Fig. 1(a). As for Al-deficient $(\text{Ta,Al})\text{B}_2$, DOS of $\text{Ta}_{0.5}\text{Al}_{0.5-\mu}\text{Va}_\mu\text{B}_2$ with $\mu = 0.083$ and 0.167, and $\text{Ta}_{0.6}\text{Al}_{0.4-\mu}\text{Va}_\mu\text{B}_2$ with $\mu = 0.1$ are shown in Figs. 5(b) and 5(c). Our results reveal a minor shift of the Fermi level towards the pseudogap because of the presence of Al vacancies, indicating not only the reduction of the number of electrons occupying the antibonding states but also the associated improvement in the stability of the solid solutions. However, an excessive number of vacancies in the system may eventually lead to the partial removal of electrons occupying the bonding states and/or an increase in the number of broken bonds around the vacancies, thus destabilizing the materials [14, 15, 17].

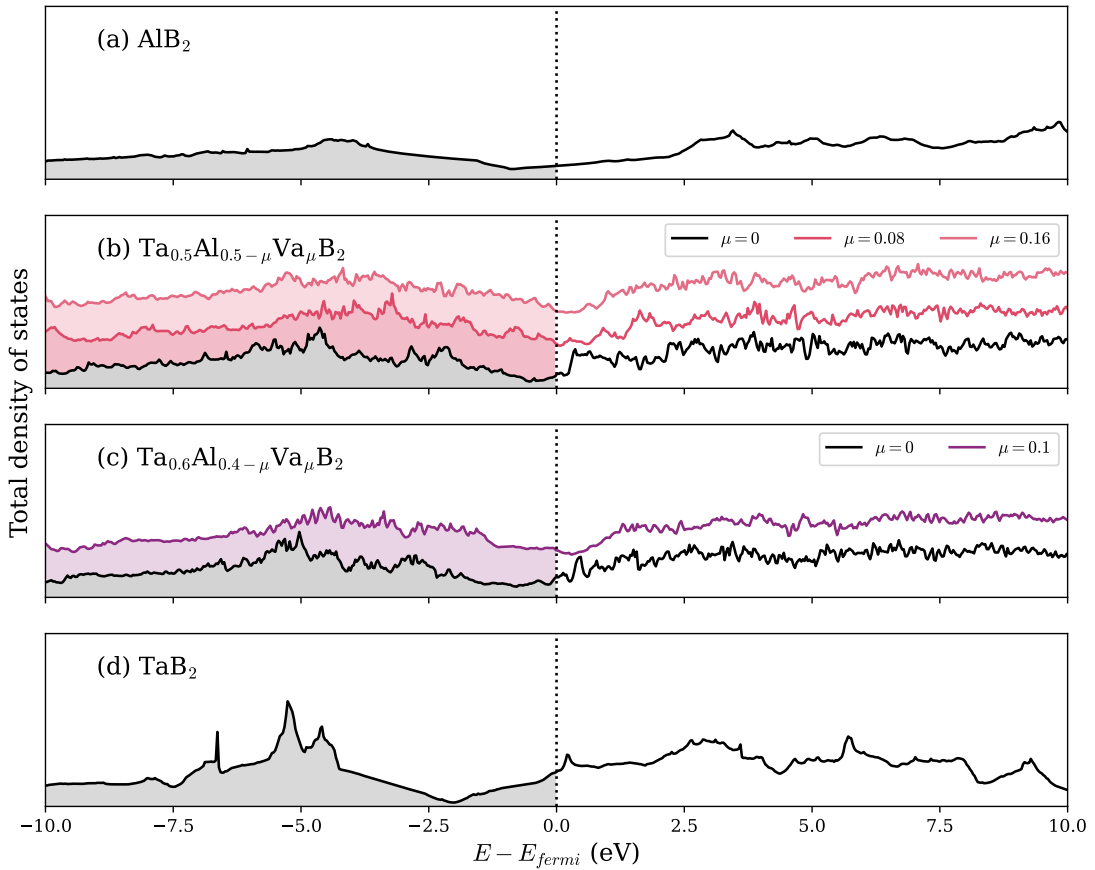


FIG. 5: (a)–(d) Total electronic density of states (DOS) of $\text{Ta}_x\text{Al}_{1-x}\text{B}_2$ where $x = 0, 0.5, 0.6, 1$, represented by the black lines. The stacking lines in (b) and (c) represent DOS of $\text{Ta}_{0.5}\text{Al}_{0.5-\mu}\text{Va}_{\mu}\text{B}_2$ with $\mu = 0.083, 0.167$ (red lines) and $\text{Ta}_{0.6}\text{Al}_{0.4-\mu}\text{Va}_{\mu}\text{B}_2$ with $\mu = 0.1$ (purple line). The filled colors indicate the states that are occupied by electrons and the vertical dashed lines at 0 eV represent the Fermi level.

E. Elastic properties of Al-deficient (Ta,Al) B_2

Apart from its influences on the stability as well as the structural and electronic properties, the introduction of Al vacancies on the metal sublattice is expected to play an important role in altering the elastic properties as well as the hardness of (Ta,Al) B_2 solid solutions. Given the relevance of these properties for potential hard-coating applications, we have provided in Table II our calculated key elastic characteristics for TaB_2 , AlB_2 , (Ta,Al) B_2 , and Al-deficient (Ta,Al) B_2 in comparison to the theoretical and experimental data reported in other works [2, 3, 7, 15, 18, 44–47]. Moreover, the trends of changes in bulk modulus, shear modulus, Young’s modulus, and hardness, as the vacancy concentration μ increases from 0 to 0.167, are illustrated in Fig. 6. Our calculated \bar{C}_{ij} , elastic moduli and hardness for TaB_2 exhibit good agreement with the theoretical data of TaB_2 , previously reported in the literature [3, 7, 18, 45]. The calculated elastic moduli and hardness of TaB_2 also align quite well with those measured from the experimentally synthesized

bulk TaB_2 [2, 16, 46, 47]; however, as shown in Ref. [15], the calculated elastic moduli of TaB_2 can further be more consistent with the existing experimental data if the B vacancies are taken into account in the structural model of the diboride. On the other hand, the calculated elastic properties of AlB_2 (and also Al-deficient AlB_2) have not been extensively examined with relatively few reports available in the theoretical literature [18, 44, 45].

For the ordered solid solution of $\text{Ta}_{0.5}\text{Al}_{0.5}\text{B}_2$ ($\text{Ta}_{0.6}\text{Al}_{0.4}\text{B}_2$), we found a decrease in the bulk, shear, and Young’s moduli of approximately 22.5% (17.8%), 14.8% (9.4%), and 16.3% (11.0%), respectively, as compared to those of stoichiometric TaB_2 . The decreases in their elastic moduli primarily stem from reductions in most \bar{C}_{ij} . Nevertheless, we noticed a slight increase in the hardness values of around 2.0% (6.5%), relative the that of TaB_2 . Also, our theoretically derived value of hardness of the ordered $\text{Ta}_{0.5}\text{Al}_{0.5}\text{B}_2$ was found to be higher than that of the disordered $\text{Ta}_{0.5}\text{Al}_{0.5}\text{B}_2$, predicted by Šroba *et al* [18], by 11.8%. Additionally, the B/G ratio of the solid solutions was observed to decrease slightly

TABLE II: Projected hexagonal elastic constants (\bar{C}_{ij}), bulk modulus (B), shear modulus (G), Young's modulus (E), hardness (H), and B/G ratio of AlB_2 , $\text{Ta}_{0.5}\text{Al}_{0.5}\text{B}_2$, $\text{Ta}_{0.5}\text{Al}_{0.417}\text{Va}_{0.083}\text{B}_2$, $\text{Ta}_{0.5}\text{Al}_{0.333}\text{Va}_{0.167}\text{B}_2$, $\text{Ta}_{0.6}\text{Al}_{0.4}\text{B}_2$, $\text{Ta}_{0.6}\text{Al}_{0.3}\text{Va}_{0.1}\text{B}_2$, and TaB_2 . A comparison is conducted with existing experimental and theoretical data on the elastic properties of AlB_2 and TaB_2 found in the literature.

Composition	Elastic constants \bar{C}_{ij} (GPa)						Elastic moduli (GPa), Hardness (GPa) and B/G ratio					
	\bar{C}_{11}	\bar{C}_{12}	\bar{C}_{13}	\bar{C}_{33}	\bar{C}_{44}	\bar{C}_{66}	B	G	E	H	B/G	Ref.
AlB_2	558.2	101.7	2.1	389.5	48.4	228.2	185.3	125.0	306.1	18.3	1.5	This work
	665.0	41.0	17.0	417.0	58.0	-	205.2	105.4	269.9	-	2.0	Calc.[44]
	522.0	75.0	79.0	255.0	32.0	-	190.5	95.0	244.4	-	2.0	Calc.[45]
	-	-	-	-	-	-	175.7	107.0	266.8	14.2	1.6	Calc.[18]
$\text{Ta}_{0.5}\text{Al}_{0.5}\text{B}_2$	553.7	157.3	105.5	387.1	156.2	198.2	243.0	175.5	424.3	25.1	1.4	This work
$\text{Ta}_{0.5}\text{Al}_{0.417}\text{Va}_{0.083}\text{B}_2$	570.3	130.4	109.6	402.2	163.7	220.0	245.4	186.7	446.9	28.0	1.3	This work
$\text{Ta}_{0.5}\text{Al}_{0.333}\text{Va}_{0.167}\text{B}_2$	588.0	107.8	103.5	417.7	152.6	240.1	244.0	190.0	452.5	29.1	1.3	This work
$\text{Ta}_{0.6}\text{Al}_{0.4}\text{B}_2$	567.6	149.4	130.2	399.9	178.3	209.1	257.7	186.7	451.2	26.2	1.4	This work
$\text{Ta}_{0.6}\text{Al}_{0.3}\text{Va}_{0.1}\text{B}_2$	580.2	127.6	131.2	415.0	199.5	226.3	258.8	202.4	481.6	30.5	1.3	This work
TaB_2	611.1	140.2	216.2	460.8	224.8	235.4	313.5	206.1	507.2	24.6	1.5	This work
	598.0	145.0	214.0	442.0	208.0	227.0	308.0	219.0	531.0	27.2	1.4	Calc.[3]
	596.5	138.5	193.1	427.2	188.7	229.0	294.8	190.5	470.2	22.9	1.5	Calc.[7]
	597.0	140.0	196.0	433.0	191.0	-	295.8	191.5	472.5	-	1.5	Calc.[45]
$\text{TaB}_{\sim 2}$	-	-	-	-	-	-	288.8	195.0	477.5	24.6	1.5	Calc.[18]
	-	-	-	-	-	-	-	228.0 \pm 3.0	551.0 \pm 3.0	25.6 \pm 0.7	-	Expt.[2]
	-	-	-	-	-	-	-	-	-	22.3–29.2	-	Expt.[16]
	-	-	-	-	-	-	-	-	-	24.7	-	Expt.[46]
$\text{TaB}_{1.833}$	615.5	126.3	188.0	534.2	259.3	244.6	307.7	234.4	560.7	32.4	1.3	Calc.[15]
	609.3	127.2	182.8	546.7	264.0	241.0	305.6	236.5	564.0	33.3	1.3	Calc.[15]
	599.6	126.5	180.0	554.8	268.5	236.5	303.0	237.0	564.1	33.8	1.3	Calc.[15]
	-	-	-	-	-	-	-	-	-	24.5	-	Expt.[47]

with respect to that of TaB_2 , indicating the increase in brittleness of the solid solutions relative to TaB_2 . Overall, alloying TaB_2 with AlB_2 led to a reduction in most of the elastic constants \bar{C}_{ij} and moduli with a slight increase in the hardness and the degree of brittleness with respect to those of TaB_2 .

By investigating the influences of Al vacancies on the elastic properties of $(\text{Ta,Al})\text{B}_2$, an enhancement in the elastic properties of Al-deficient $(\text{Ta,Al})\text{B}_2$ relative to those of $(\text{Ta,Al})\text{B}_2$ was evidently observed, except the bulk modulus remaining relatively constant at ~ 244 GPa and ~ 258 GPa for $\text{Ta}_{0.5}\text{Al}_{0.5-\mu}\text{Va}_{\mu}\text{B}_2$ and $\text{Ta}_{0.6}\text{Al}_{0.4-\mu}\text{Va}_{\mu}\text{B}_2$ where $0 \leq \mu \leq 0.167$, respectively, as can be seen from Fig. 6(a). As depicted in Fig. 6(b) and 6(c), the shear and Young's moduli of $\text{Ta}_{0.5}\text{Al}_{0.5-\mu}\text{Va}_{\mu}\text{B}_2$ where $\mu = 0.083$ (0.167) showed a slight increase by 6.4% (8.3%) and 5.3% (6.6%), respectively, as compared to those of the ordered $\text{Ta}_{0.5}\text{Al}_{0.5}\text{B}_2$ without the presence of Al vacancies ($\mu = 0$).

Similarly, for $\text{Ta}_{0.6}\text{Al}_{0.3}\text{Va}_{0.1}\text{B}_2$, the shear and Young's moduli increased by 8.4% and 6.7% respectively as compared to those of ordered and vacancy-free $\text{Ta}_{0.6}\text{Al}_{0.4}\text{B}_2$, see also Fig. 6(b) and 6(c). These improvements in the shear and Young's moduli of Al-deficient $(\text{Ta,Al})\text{B}_2$ with respect to those of vacancy-free $(\text{Ta,Al})\text{B}_2$ can directly

be attributed to the reduction in the number of electrons occupying the antibonding states induced by the partial substitution of vacancies for Al atoms residing on the metal sublattice, as already discussed in Ref. [14] and in Section III D of the present work. Consequently, such increases in the values of the shear modulus as well as the roughly constant bulk modulus result in an enhancement of the hardness of $\text{Ta}_{0.5}\text{Al}_{0.5-\mu}\text{Va}_{\mu}\text{B}_2$ where $\mu = 0.083$ (0.167) by 11.6% (15.9%) and $\text{Ta}_{0.6}\text{Al}_{0.3}\text{Va}_{0.1}\text{B}_2$ by 16.4% as compared to those of the vacancy-free solid solutions (see Fig. 6(d)). Conversely, the reductions in the value of B/G ratio were found for Al-deficient $(\text{Ta,Al})\text{B}_2$ compared to the vacancy-free solid solutions, indicating an increase in brittleness due to the presence of Al vacancies. It would, however, be good to note that, although these hardness values of Al-deficient $(\text{Ta,Al})\text{B}_2$, according to our predictions, potentially surpass that of TaB_2 , for example, $\text{Ta}_{0.6}\text{Al}_{0.3}\text{Va}_{0.1}\text{B}_2$ with the hardness of 30.5 GPa, it is 9.8% lower than the hardness of B-deficient $\text{TaB}_{2-\delta}$ (with $\delta = 0.25$).

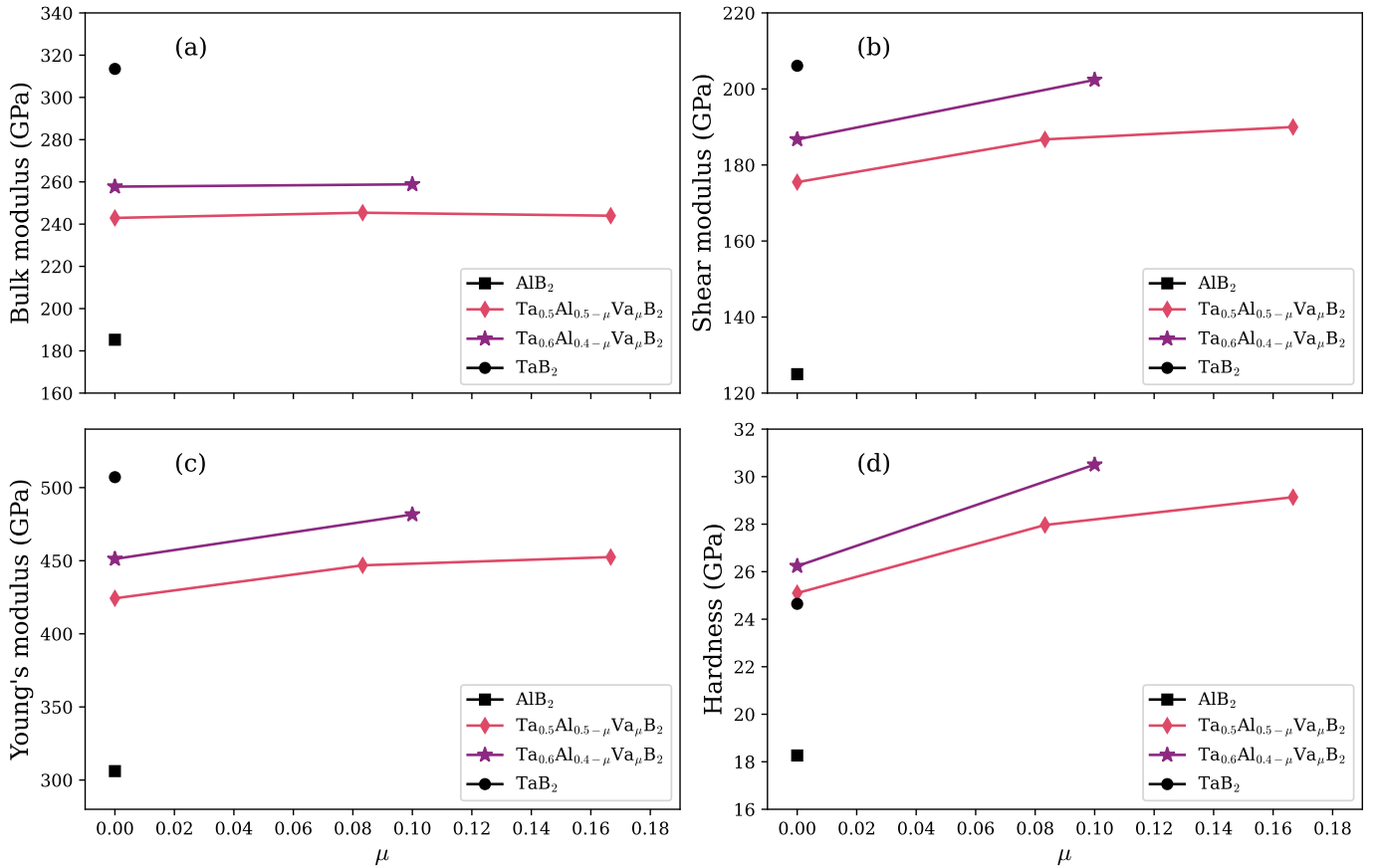


FIG. 6: (a) Bulk modulus, (b) shear modulus, (c) Young's modulus, and (d) hardness in GPa of AlB_2 (black squares), $\text{Ta}_{0.5}\text{Al}_{0.5-\mu}\text{Va}_\mu\text{B}_2$ with $\mu = 0, 0.083, 0.167$ (red diamonds), $\text{Ta}_{0.6}\text{Al}_{0.4-\mu}\text{Va}_\mu\text{B}_2$ with $\mu = 0.1$ (purple stars), and TaB_2 (black circles), respectively.

IV. CONCLUSION

In summary, our work provides comprehensive insights into the thermodynamic stability, as well as the structural, electronic, and elastic properties of $(\text{Ta},\text{Al})\text{B}_2$ and Al-deficient $(\text{Ta},\text{Al})\text{B}_2$ alloys. The investigation was done by employing first-principles calculations with the aim of addressing the key questions raised in the introduction. Firstly, we demonstrated how the introduction of Al atoms into TaB_2 induces changes in lattice parameters and the electronic density of state, primarily driven by a decrease in the occupancy of electrons in the antibonding states. While most elastic properties of the resulting solid solutions exhibit a slight deterioration with respect to those of TaB_2 , there is a marginal enhancement in their hardness. Furthermore, despite exhibiting negative mixing energies across various compositions compared to TaB_2 and AlB_2 , $(\text{Ta},\text{Al})\text{B}_2$ solid solutions, all without the presence of any structural defects are found to be thermodynamically unstable relative to all relevant competing phases at absolute zero in Ta–Al–B system.

Our calculations also indicate a preference for partial substitution of vacancies for Al atoms in the $(\text{Ta},\text{Al})\text{B}_2$. Through the thermodynamic consideration of different compositions and configurations of Al-deficient $(\text{Ta},\text{Al})\text{B}_2$, we identified $\text{Ta}_{0.6}\text{Al}_{0.3}\text{B}_2$ as one of the stable phases in the Ta–Al–B system. The presence of vacancies significantly contributes to the increase in stability via the reason of electronic band filling. Our predicted stable composition of Al-deficient $(\text{Ta},\text{Al})\text{B}_2$ as well as the newly proposed ternary ground-state diagram of the Ta–Al–B system demonstrate reasonable agreement between theoretical predictions and experimental observations, indicating a tendency for $(\text{Ta},\text{Al})\text{B}_2$ solid solutions to undergo phase separation into their relevant competing phases, such as face-centered cubic Al, Al-deficient $\text{Ta}_{0.6}\text{Al}_{0.3}\text{B}_2$, and B-deficient $\text{TaB}_{2-\delta}$. Although the elastic properties as well as the hardness of $(\text{Ta},\text{Al})\text{B}_2$ solid solutions can, for a given Ta content, be enhanced due to the partial substitution of vacancies for Al atoms in the solutions, they are unfortunately inferior to those of B-deficient $\text{TaB}_{2-\delta}$.

V. ACKNOWLEDGMENTS

This research project is supported by (1) Thailand Science Research and Innovation Fund Chulalongkorn University, (2) the Asahi Glass Foundation (RES_66_104_2300_016), (3) Sci-Super X fund, Faculty of Science, Chulalongkorn University, and (4) the NSRF via the Program Management Unit for Human Resources & Institutional Development, Research and Innovation (Grant No. B37G660011). B.A. acknowledges the financial support from the Swedish Research Council (VR) through Grant No. 2019-05403, and 2023-05194 from the Swedish Government Strategic Research Area in Materials Science on Functional Materials at Linköping University (Faculty Grant SFOMatLiU No. 2009-00971). The computations were enabled by resources provided by the National Academic Infrastructure for Supercomputing in Sweden (NAISS) partially funded by the Swedish Research Council through grant agreement no. 2022-06725.

* Electronic address: Annop.E@chula.ac.th

- [1] I. R. Shein, A. L. Ivanovskii, Elastic properties of mono- and polycrystalline hexagonal AlB_2 -like diborides of s, p and d metals from first-principles calculations, *Journal of Physics: Condensed Matter* 20 (41) (2008) 415218.
- [2] X. Zhang, G. E. Hilmas, W. G. Fahrenholtz, Synthesis, densification, and mechanical properties of TaB_2 , *Materials Letters* 62 (27) (2008) 4251–4253.
- [3] W. J. Zhao, Y. X. Wang, Structural, mechanical, and electronic properties of TaB_2 , TaB , IrB_2 , and IrB : First-principle calculations, *Journal of Solid State Chemistry* 182 (10) (2009) 2880–2886.
- [4] M. B. Weinberger, J. B. Levine, H.-Y. Chung, R. W. Cumberland, H. I. Rasool, J.-M. Yang, R. B. Kaner, S. H. Tolbert, Incompressibility and hardness of solid solution transition metal diborides: $Os_{1-x}Ru_xB_2$, *Chemistry of Materials* 21 (9) (2009) 1915–1921.
- [5] B. Alling, H. Högborg, R. Armiento, J. Rosén, L. Hultman, A theoretical investigation of mixing thermodynamics, age-hardening potential and electronic structure of ternary $M1_{1-x}M2_xB_2$ alloys with AlB_2 type structure, *Scientific reports* 5 (1) (2015) 9888.
- [6] N. Nedfors, S. Mráz, J. Palisaitis, P. O. Persson, H. Lind, S. Kolozsvari, J. M. Schneider, J. Rosen, Influence of the Al concentration in Ti-Al-B coatings on microstructure and mechanical properties using combinatorial sputtering from a segmented TiB_2/AlB_2 target, *Surface and Coatings Technology* 364 (2019) 89–98.
- [7] Z. Mai, X. Zhang, Y. Liu, H. Yu, F. Wang, Insight into the structure dependence on physical properties of the high temperature ceramics TaB_2 boride, *Vacuum* 177 (2020) 109427.
- [8] B. Bakhit, J. Palisaitis, J. Thörnberg, J. Rosen, P. O. Persson, L. Hultman, I. Petrov, J. E. Greene, G. Greczynski, Improving the high-temperature oxidation resistance of TiB_2 thin films by alloying with Al, *Acta Materialia* 196 (2020) 677–689.
- [9] E. Johansson, A. Ektarawong, J. Rosen, B. Alling, Theoretical investigation of mixing and clustering thermodynamics of $Ti_{1-x}Al_xB_2$ alloys with potential for age-hardening, *Journal of Applied Physics* 128 (23) (2020).
- [10] B. Bakhit, S. Dorri, A. Kooijman, Z. Wu, J. Lu, J. Rosen, J. M. Mol, L. Hultman, I. Petrov, J. E. Greene, et al., Multifunctional ZrB_2 -rich $Zr_{1-x}Cr_xB_y$ thin films with enhanced mechanical, oxidation, and corrosion properties, *Vacuum* 185 (2021) 109990.
- [11] K. Mopoung, A. Ektarawong, T. Pakornchote, E. Johansson, B. Alling, Effect of chemical composition and atomic configuration on thermodynamic stability and elastic properties of AlB_2 -type $Sc_{1-x}V_xB_2$ solid solutions: A first-principles investigation, *Computational Materials Science* 213 (2022) 111616.
- [12] X. Gu, C. Liu, X. Gao, K. Zhang, W. Zheng, C. Chen, Solving strength–toughness dilemma in superhard transition-metal diborides via a distinct chemically tuned solid solution approach, *Research* 6 (2023) 0035.
- [13] K. Mopoung, A. Ektarawong, T. Bovornratanaraks, B. Alling, First-principles demonstration of band filling-induced significant improvement in thermodynamic stability and mechanical properties of $Sc_{1-x}Ta_xB_2$ solid solutions, *Scientific Reports* 13 (1) (2023) 10504.
- [14] M. Dahlqvist, J. Rosen, Impact of vacancies on structure, stability and properties of hexagonal transition metal diborides, MB_2 (M= Sc, Y, Ti, Zr, Hf, V, Nb, Ta, Cr, Mo, W, Mn, and Fe), *Materialia* 26 (2022) 101629.
- [15] A. Ektarawong, E. Johansson, T. Pakornchote, T. Bovornratanaraks, B. Alling, Boron vacancy-driven thermodynamic stabilization and improved mechanical properties of AlB_2 -type tantalum diborides as revealed by first-principles calculations, *Journal of Physics: Materials* 6 (2) (2023) 025002.
- [16] S. Otani, M. Korsukova, T. Mitsuhashi, Floating zone growth and high-temperature hardness of NbB_2 and TaB_2 single crystals, *Journal of crystal growth* 194 (3–4) (1998) 430–433.
- [17] E. Johansson, F. Eriksson, A. Ektarawong, J. Rosen, B. Alling, Coupling of lattice dynamics and configurational disorder in metal deficient $Al_{1-\delta}B_2$ from first-principles, *Journal of Applied Physics* 130 (1) (2021).
- [18] V. Šroba, T. Fiantok, M. Truchlý, T. Roch, B. Grančič, K. Viskupová, L. Satrapinsky, P. Švec, Š. Nagy, V. Izai, et al., Structure evolution and mechanical properties of Al-alloyed tantalum diboride films prepared by magnetron sputtering co-deposition, *Journal of Vacuum Science & Technology A* 41 (2) (2023).
- [19] P. Hohenberg, W. Kohn, Inhomogeneous electron gas, *Physical review* 136 (3B) (1964) B864.
- [20] W. Kohn, L. J. Sham, Self-consistent equations including exchange and correlation effects, *Physical review* 140 (4A) (1965) A1133.
- [21] J. M. Sanchez, F. Ducastelle, D. Gratias, Generalized cluster description of multicomponent systems, *Physica A: Statistical Mechanics and its Applications* 128 (1-2) (1984) 334–350.
- [22] L. Ferreira, S.-H. Wei, A. Zunger, First-principles calculation of alloy phase diagrams: The renormalized-interaction approach, *Physical Review B* 40 (5) (1989) 3197.
- [23] G. L. Hart, R. W. Forcade, Algorithm for generating derivative structures, *Physical Review B* 77 (22) (2008)

- 224115.
- [24] M. Ångqvist, W. A. Muñoz, J. M. Rahm, E. Fransson, C. Durniak, P. Rozyczko, T. H. Rod, P. Erhart, Icet—a python library for constructing and sampling alloy cluster expansions, *Advanced Theory and Simulations* 2 (7) (2019) 1900015.
- [25] G. Kresse, J. Furthmüller, Efficiency of ab-initio total energy calculations for metals and semiconductors using a plane-wave basis set, *Computational materials science* 6 (1) (1996) 15–50.
- [26] G. Kresse, J. Furthmüller, Efficient iterative schemes for ab initio total-energy calculations using a plane-wave basis set, *Physical review B* 54 (16) (1996) 11169.
- [27] G. Kresse, D. Joubert, From ultrasoft pseudopotentials to the projector augmented-wave method, *Physical review B* 59 (3) (1999) 1758.
- [28] D. Hobbs, G. Kresse, J. Hafner, Fully unconstrained noncollinear magnetism within the projector augmented-wave method, *Physical Review B* 62 (17) (2000) 11556.
- [29] J. P. Perdew, K. Burke, M. Ernzerhof, Generalized gradient approximation made simple, *Physical review letters* 77 (18) (1996) 3865.
- [30] H. J. Monkhorst, J. D. Pack, Special points for Brillouin-zone integrations, *Physical review B* 13 (12) (1976) 5188.
- [31] P. E. Blöchl, O. Jepsen, O. K. Andersen, Improved tetrahedron method for Brillouin-zone integrations, *Physical Review B* 49 (23) (1994) 16223.
- [32] C. Atthapak, A. Ektarawong, T. Pakornchote, B. Alling, T. Bovornratanaraks, Effect of atomic configuration and spin–orbit coupling on thermodynamic stability and electronic bandgap of monolayer $2\text{H-Mo}_{1-x}\text{W}_x\text{S}_2$ solid solutions, *Physical Chemistry Chemical Physics* 23 (24) (2021) 13535–13543.
- [33] A. Van De Walle, Multicomponent multisublattice alloys, nonconfigurational entropy and other additions to the Alloy Theoretic Automated Toolkit, *Calphad* 33 (2) (2009) 266–278.
- [34] L. Barroso-Luque, P. Zhong, J. H. Yang, F. Xie, T. Chen, B. Ouyang, G. Ceder, Cluster expansions of multicomponent ionic materials: Formalism and methodology, *Physical Review B* 106 (14) (2022) 144202.
- [35] C. Atthapak, A. Ektarawong, T. Pakornchote, B. Alling, T. Bovornratanaraks, Thermodynamic stability prediction of triple transition-metals $(\text{Ti-Mo-V})_3\text{C}_2$ MXenes via cluster correlation-based machine learning (accepted for publication in *Advanced Theory and Simulations*) (2024).
- [36] F. Pedregosa, G. Varoquaux, A. Gramfort, V. Michel, B. Thirion, O. Grisel, M. Blondel, P. Prettenhofer, R. Weiss, V. Dubourg, et al., Scikit-learn: Machine learning in python, the *Journal of machine Learning research* 12 (2011) 2825–2830.
- [37] R. Golezorkhtabar, P. Pavone, J. Spitaler, P. Puschnig, C. Draxl, Elastic: A tool for calculating second-order elastic constants from first principles, *Computer Physics Communications* 184 (8) (2013) 1861–1873.
- [38] M. Moakher, A. N. Norris, The closest elastic tensor of arbitrary symmetry to an elasticity tensor of lower symmetry, *Journal of Elasticity* 85 (2006) 215–263.
- [39] F. Mouhat, F.-X. Coudert, Necessary and sufficient elastic stability conditions in various crystal systems, *Physical review B* 90 (22) (2014) 224104.
- [40] G. Simmons, H. Wang, *Single crystal elastic constants and calculated aggregate properties: a handbook*, (No Title) (1971).
- [41] X.-Q. Chen, H. Niu, D. Li, Y. Li, Modeling hardness of polycrystalline materials and bulk metallic glasses, *Intermetallics* 19 (9) (2011) 1275–1281.
- [42] A. Ivanovskii, Hardness of hexagonal AlB₂-like diborides of s, p and d metals from semi-empirical estimations, *International Journal of Refractory Metals and Hard Materials* 36 (2013) 179–182.
- [43] S. Pugh, Xcii. relations between the elastic moduli and the plastic properties of polycrystalline pure metals, *The London, Edinburgh, and Dublin Philosophical Magazine and Journal of Science* 45 (367) (1954) 823–843.
- [44] K. Liu, X.-L. Zhou, X.-R. Chen, W.-J. Zhu, Structural and elastic properties of AlB₂ compound via first-principles calculations, *Physica B: Condensed Matter* 388 (1-2) (2007) 213–218.
- [45] Y. Duan, Y. Sun, Z. Guo, M. Peng, P. Zhu, J. He, Elastic constants of AlB₂-type compounds from first-principles calculations, *Computational materials science* 51 (1) (2012) 112–116.
- [46] R. Chuzhko, O. Balakhovskii, A. Vorotnikov, Temperature dependence of the hardness of diffusion coatings of Ta₂C and TaB₂, *Metal Science and Heat Treatment* 19 (1977) 60–61.
- [47] J. J. Gilman, *Chemistry and physics of mechanical hardness*, John Wiley & Sons, 2009.

Supporting Information

Role of Al vacancies in thermodynamic stability and elastic properties of AlB_2 -type $(\text{Ta,Al})\text{B}_2$: A first-principles study

A. Ektarawong,^{1, 2, 3, *} C. Atthapak,^{1, 2} and B. Alling⁴

¹Extreme Conditions Physics Research Laboratory and Center of Excellence in Physics of Energy Materials (CE:PEM), Department of Physics, Faculty of Science, Chulalongkorn University, Bangkok 10330, Thailand

²Thailand Center of Excellence in Physics, Ministry of Higher Education, Science, Research and Innovation, 328 Si Ayutthaya Road, Bangkok 10400, Thailand

³Chula Intelligent and Complex Systems, Department of Physics, Faculty of Science, Chulalongkorn University, Bangkok 10330, Thailand

⁴Theoretical Physics Division, Department of Physics, Chemistry and Biology (IFM), Linköping University, SE-581 83, Linköping, Sweden

*Electronic address: Annop.E@chula.ac.th

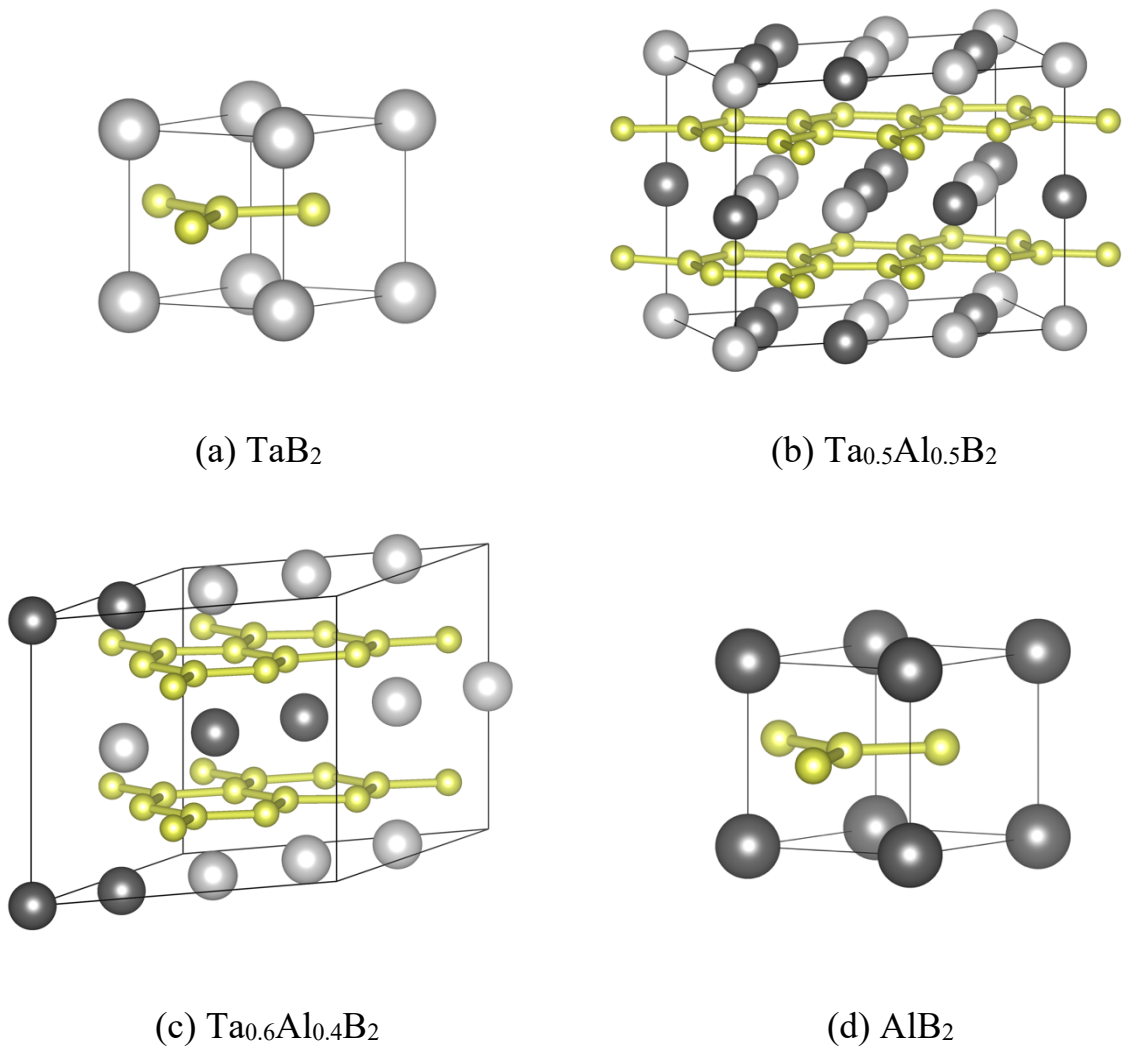
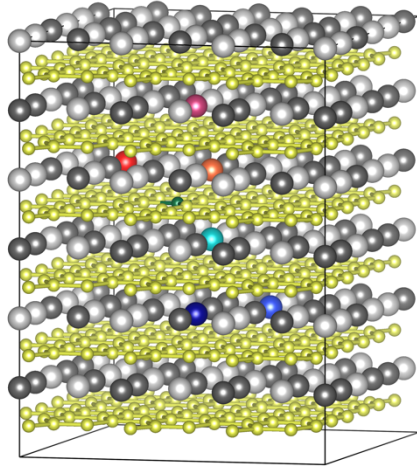
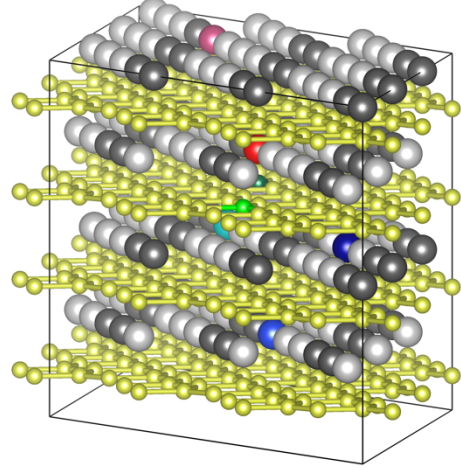


Figure S1. Visualization of four candidates for ground-state configurations of $\text{Ta}_x \text{Al}_{1-x}\text{B}_2$, where $0 \leq x \leq 1$, consisting of (a) TaB_2 , (b) $\text{Ta}_{0.5}\text{Al}_{0.5}\text{B}_2$, (c) $\text{Ta}_{0.6}\text{Al}_{0.4}\text{B}_2$, and (d) AlB_2 , which are obtained from the convex hull in Fig. 1. Large gray, large dark gray, and small yellow spheres represent Ta, Al, and B atoms, respectively.



(a) $\text{Ta}_{0.5}\text{Al}_{0.5}\text{B}_2$



(b) $\text{Ta}_{0.6}\text{Al}_{0.4}\text{B}_2$

Figure S2. Visualization of (a) $3 \times 3 \times 2$ supercell (648 atoms) of $\text{Ta}_{0.5}\text{Al}_{0.5}\text{B}_2$ and (b) $3 \times 3 \times 2$ supercell (540 atoms) of $\text{Ta}_{0.6}\text{Al}_{0.4}\text{B}_2$. In the visualizations, large gray, large dark gray, and small yellow spheres represent lattice sites of Ta, Al, and B atoms, respectively. Large red, pink, and orange (sky blue, blue, and dark blue) spheres denote inequivalent crystallographic sites of Al(Ta) atoms, namely, Al(1), Al(2), and Al(3) (Ta(1), Ta(2), and Ta(3)) sites, respectively. Small green and lime spheres denote inequivalent crystallographic sites of B atoms, namely, B(1) and B(2) sites. These sites are considered for estimating formation energies of a single Al, Ta, or B vacancy in the dilute limit as listed in Table 1.

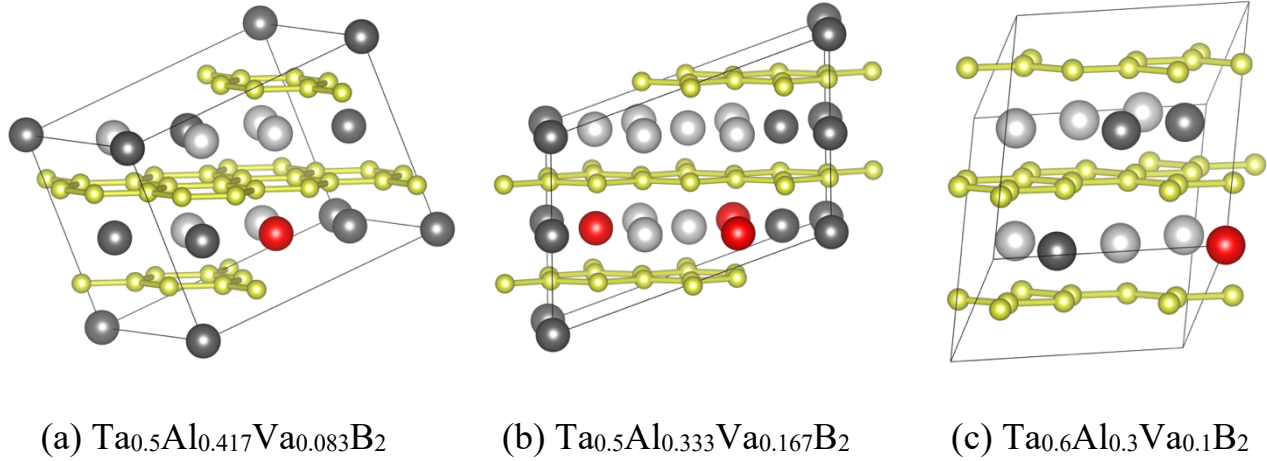


Figure S3. Visualization of candidates for ground-state configurations of Al-deficient (Ta,Al) B_2 . (a) $\text{Ta}_{0.5}\text{Al}_{0.417}\text{Va}_{0.083}\text{B}_2$ and (b) $\text{Ta}_{0.5}\text{Al}_{0.333}\text{Va}_{0.167}\text{B}_2$ are obtained from the convex hull in Fig. 2(a), whereas (c) $\text{Ta}_{0.6}\text{Al}_{0.3}\text{Va}_{0.1}\text{B}_2$ is obtained from the ground-state configuration in Fig. 2(b). Large gray, large dark gray, and small yellow (large red) spheres represent Ta, Al, and B atoms (Al vacancies), respectively.

TABLE S1. Formation energies (E_f) and energies above the Ta-Al-B convex hull in Figure 3 (E_{ab}) of different prototypes of stoichiometric TaB_2 .

Phase	Pearson symbol	Space group	E_f (eV/atom)	E_{ab} (meV/atom)
Al B_2 -type	hP3	$P6/mmm$	-0.654	22
W B_2 -type	hP12	$P6_3/mmc$	-0.669	7
Mo B_2 -type	hR18	$R\bar{3}m$	-0.663	13
Re B_2 -type	hP6	$P6_3/mmc$	-0.267	408
Ru B_2 -type	oP6	$Pm\bar{m}n$	-0.305	370
Fe B_2 -type	oP12	$Pnma$	-0.204	471
Mn B_2 -type	oI18	$Im\bar{m}m$	-0.435	240